RSC Publishing Faraday Discussions

The Impact of Optically Rectified Fields on Plasmonic Electrocatalysis

Journal:	*Faraday Discussions*
Manuscript ID	FD-ART-09-2018-000135.R1
Article Type:	Paper
Date Submitted by the Author:	03-Nov-2018
Complete List of Authors:	Nelson, Darby; The Ohio State University Schultz, Zachary; The Ohio State University

The Impact of Optically Rectified Fields on Plasmonic Electrocatalysis.

Darby A. Nelson, and Zachary D. Schultz*

The Ohio State University, Department of Chemistry & Biochemistry, Columbus, OH, 43210, USA

*email of corresponding author: Schultz.133@osu.edu

ABSTRACT

Studies have shown the excitation of plasmon resonances on nanostructured materials can drive catalytic processes. Plasmon resonances can be tuned across the solar spectrum, offering intriguing application possibilities for plasmonic catalysis. Previous work in our group indicates that nanostructures with tight junctions can create direct current (DC) electric fields. These fields arise from an optical rectification of the plasmon resonance on the plasmonic surface, and our group has shown these fields modulate photocatalytic activity. This work looks to shed further light on the impact optically rectified fields can have on catalytic reactions. Cyclic voltammetry shows that the electrochemical reduction and oxidation potentials of a 2 mM $CuSO_4$ solution occur at ~100 mV lower overpotential on an optically excited Ag nanodendrite electrode. Stark spectroscopy of nitriles absorbed to these surfaces indicate photo-associated changes in surface potential across the Ag nanodendrites. Localized areas evince photo-induced changes in surface potential upwards of 300 mV. These results provide evidence of optically rectified fields altering electrochemical reactivity on plasmonic surfaces and suggest optimizing this nonlinear phenomenon may improve plasmonic photocatalysts.

INTRODUCTION

Reports have shown that the excitation of electrons in localized surface plasmon resonances (LSPR) can drive photocatalytic reactions on plasmonic materials.[1-3] In fact, the ability to tune the LSPR across the solar spectrum offers tremendous possibilities for photocatalysis. Plasmonic nanostructures promote chemical reactions on their surfaces when illuminated at their plasmon resonance frequency.[1, 2, 4-7] This behavior is contrary to that traditionally observed on bulk surfaces of the same materials that do not support catalysis. These catalysts are commonly made of metals that have intra-band electronic transitions. The frequency dependence of the increased reactivity correlates strongly with the plasmon resonance rather than the electronic transition, thus further implicating a plasmonic effect. Interestingly, the excitation of plasmon resonances has been reported to alter the selectivity of reaction products.[8, 9] Increased understanding of the phenomena arising from plasmon resonances offers tremendous potential for new photocatalysts.

On nanostructured arrays, heterogeneous reactivity has been observed, implicating "hotspots" and step-edges, areas of intense electric fields, are important for catalysis.[10, 11] The excitation of localized surface plasmon resonances in metal nanostructures results in confined electric fields that are commonly utilized for chemical transformation and trace detection.[1, 12, 13 14-16] These electric fields are largely responsible for signal enhancements in surface related spectroscopies, where the optical response of molecules that experience the enhanced electromagnetic fields increases. When incident light is resonant with plasmon resonances in nanomaterials, relaxation of the excited electrons can occur both through light scattering and by thermal relaxation to produce hot electrons. These hot electrons are commonly associated with chemical transformations, such as photocatalysis, where exciting plasmon resonances facilitate chemical reactions on the nanostructure surface[1, 2, 4-7]

The role of plasmons in catalysis remains an open question. Relaxation of the electrons excited by plasmon resonances can occur through different mechanisms that lead to physical effects such as heating, hot electron formation, and optical signal generation.[1, 6, 14, 15] Electron relaxation via thermal relaxation can produce sizable temperature increases on the surface of nanoparticles depending on the thermal conductivity of the surroundings;[17] however, the role of temperature in catalysis has been recently disputed.[18] The relaxation from the excited state can form hot electrons that promote reactions near nanostructure surfaces. This hot electron mechanism has received the most attention for plasmonic catalysis.[1, 2, 4, 6]

Our lab has been exploring how exciting plasmon resonances can drive static surface potentials, as evidenced by vibrational Stark effects.[19-22] A DC field arising from plasmonic excitation was independently observed to generate a Stark shift in a molecule located in the plasmonic junction.[21, 23] Measurement of the change in vibrational frequency of the bond can thus be used to determine the magnitude of the electric field. The vibrational Stark effect has been used to measure electric fields in a variety of chemical systems including the electrochemical double layer,[24-28] proteins,[29-32] biomembranes,[33] and the energy levels of molecules.[34-36]

The vibrational Stark effect is a change in the vibrational frequency that arises from an electric field perturbation to a chemical bond. On plasmonic materials, these perturbations arise from the intense electric fields associated with excited plasmon resonances driving nonlinear optical phenomena.[37] A second order nonlinear phenomena, optical rectification appears to increase in the high field regions associated with excited plasmon resonances.[21, 23] Specifically, optical rectification results in a DC field at interfaces under the influence of high intensity electric fields as described by Equation 1:

$$V_{DC} \cong -A \cdot \chi^{(2)} \cdot E(\omega)E(\omega') \quad \text{Eq. 1}$$

In Equation 1, the DC voltage (V_{DC}) observed is related to the second order susceptibility, the electric fields [E(ω)], and a coefficient (A) accounting for the geometry of the interface.[38]

The potential (V_{DC}) induced by exciting a plasmonic junction at the resonant frequency has been determined by measuring the tunneling current through a bowtie gold electrode structure separated by a nm gap when the structure is illuminated.[37] In the bow-tie example, a bias was used across the junction to direct the optically induced current. Recent experiments in our lab show that when nanostructures have small gaps distances, within the quantum regime,[39, 40] tunneling of electrons across the junction also gives rise to a DC potential.[19] In these experiments, the dipole of the molecules in the gap biases the interface and controls the net direction of the tunneling current, which is believed to control the sign of the observed field. The vibrational Stark shift from a nitrile in this electric field can be used to determine the magnitude of the optically rectified field. Interestingly, mapping the CN stretch of a Stark reporter on a plasmonic surface shows evidence of localized regions with both net positive and negative changes in surface potential.[20]

The magnitude of the rectified field can be quite large. Apkarian and coworkers also reported optical rectification in a nanoparticle dimer giving rise to a vibrational Stark shift from a CO molecule between the two spherical particles that correlated to an electric field enhancement on the order of 10^{12} and single molecule detection.[23] The high fields reported by Apkarian and coworkers are consistent with previous work from our lab, where a 130 cm^{-1} Stark shift in the CN stretch frequency was observed from CN adsorbed onto a roughened gold surface when a nanoparticle TERS tip was brought into contact to form a plasmonic junction.[21] Only the CN in the confined region exhibits a Stark shift, while the CN stretch frequency for molecules outside the plasmonic junction is observed unchanged. Previous work investigating Stark shifts on electrochemical surfaces indicates that a blue shift corresponds to positive

potential on the metal surface, that shifts about 25 cm^{-1}/V.[24, 25, 30, 41, 42] Thus the 130 cm^{-1} Stark shifts would correspond to a change in surface potential of ~3-4V. While there remains some uncertainty, such as the distance associated with the field for the plasmonic field compared to the applied electrochemical potential, the large fields observed in these examples suggest intriguing possibilities for photocatalytic applications of nanostructures.

Recently, our lab has been able to show that the V_{DC} observed on a plasmonic Au film was able to modulate the rate of the oxidative and reductive formation of Di-mercaptoazobenzene (DMAB) from nitrothiophenol and aminothiophenol upon plasmonic excitation.[22] By using a coadsorbed Stark reporter, the surface potential was shown to correlate with changes in the rate of DMAB formation. Additionally, the photocatalytic changes were shown to correlate with electrochemically induced oxidation/reduction of the surface species.

The existence of these large DC fields on nanoparticle surfaces suggests an alternative mechanism for photocatalysis, where excitation of the LSPR in nanostructures changes the energy of the Fermi level, as evident in the vibrational Stark shift of adsorbed molecules. By providing substantial overpotential, the DC field resulting from optical rectification thus drives the chemical reaction at accelerated rates. In this report, we present results that show how the overpotential required for electrochemical reactions is modified by the optically rectified field on a plasmonic surface. We combine Stark Spectroscopy with electrochemical measurements to assess the impact of plasmon resonances on the energy required for electrochemical reactions. These results illustrate how the previously under-appreciated phenomena of optical rectification modulates the activity of plasmonic catalysts.

EXPERIMENTAL

Materials and Reagents

Silver nitrate (99%), reagent alcohol (95%), copper sulfate pentahydrate (98%), and sodium sulfate (99%) were obtained from Sigma Aldrich (Missouri, USA) and used without modification. Reynolds Wrap aluminum foil was purchased from a local hardware store (Ohio, USA) and used without modification. 4-mercaptobenzonitrile (MBN) was acquired from Synfine Research, Ltd. (Ontario, CAN) and used without modification.

Electrochemical Depositions/Measurements

Electrochemical deposition and measurements were performed with a CHI660D potentiostat. Strips of aluminum foil, with one end folded over itself multiple times to provide a sturdy surface for the alligator clip, served as the working electrode. To complete the three-electrode system, a Ag/AgCl reference electrode and platinum wire counter electrode were used. All potentials stated in the manuscript are relative to Ag/AgCl unless otherwise specified.

Photo-electrochemical measurements

All photo-electrochemical experiments were performed in a Zahner PECC-2 Cell (Admiral Instruments) with excitation occurring directly on the dendrites through a quartz window at the front of the cell. The impact of optically rectified fields on oxidation and reduction events at the surface of the Ag dendrites was measured in a solution of 2 mM Cu_2SO_4 and 100 mM Na_2SO_4. Optical excitation was achieved using 565 nm LED (Thorlabs) at a power density of 2.3 mW/mm^2.

Silver Dendrite Preparation

Silver dendrites were prepared by electrochemical deposition using a 0.05M silver nitrate solution and depositing at -1.6V for 200 seconds onto an aluminum foil working electrode. After

deposition, the dendrite/aluminum foil electrode was removed from the electrochemical cell and the dendrites were allowed to dry overnight in order to ensure they adhered to the foil.

Monolayer Preparation

A MBN monolayer was adsorbed to the surface of the Ag dendrites to generate a SERS signal. Clean Ag dendrites were soaked in a 0.01 M ethanolic solution of MBN for 24 hours to create the monolayer.

Raman Measurements

Raman spectra were acquired using a Renishaw inVia Raman microscope with a 632.8 nm HeNe laser (Thorlabs). For MBN studies, the scattering between 1912-2374 cm^{-1} was collected. Spectral analysis was performed using MATLAB with a modified peak-fitting script from Mathworks. Spectra were fit with a single Gaussian, with the optimal fit being that with the smallest percent root mean squared (RMS) error. In general, 15 iterations were sufficient to minimize the RMS error.

For experiments analyzing the changes in MBN vibrational frequency from LED exposure, a 455 nm LED (Thorlabs) was used as it provided the highest power density (5.4 mW/mm^2) to the sample without exciting at wavelengths in the Raman spectrum collection region from the 632.8 nm laser.

RESULTS AND DISCUSSION

Silver nanodendrites were prepared by electrochemical reduction of $AgNO_3$ onto aluminum foil. These structures have previously been reported to provide high surface area electrodes[43] and enable surface enhanced Raman scattering.[44] The structure of these electrodes is consistent with heterogeneous surfaces previously shown to evince Stark shifts from nitrile containing molecules adsorbed to the surface.[20] To calibrate the surface potential to the vibrational frequency of our Stark reporter molecule adsorbed to the Ag dendrites, we performed spectro-electrochemical measurements. Figure 1 shows the observed CN stretch frequency as a function of applied electrochemical potential from MBN adsorbed to the Ag nanostructures. The potential was swept from 0V to -1V at a scan rate of 10 mV/s while Raman spectra were recorded every second. As the surface potential becomes increasingly negative, the CN stretch frequency is observed to decrease to lower Raman shifts. Fitting the change in CN stretch frequency versus potential indicates a Stark tuning coefficient of 8 cm^{-1}/V. This value is consistent with our previous reports from MBN on Au nanowire array electrodes.[22]

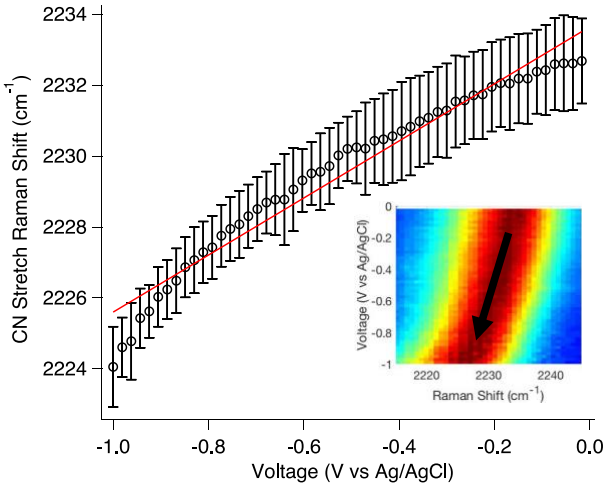

Figure 1. The change in CN stretch frequency as a function of applied electrochemical potential is plotted for MBN adsorbed to a Ag nanodendrite electrode. The CN stretch is observed to decrease at a rate of 8 cm^{-1} V^{-1}. The inset shows a heatmap illustrating how the vibrational mode lineshape evolves with potential. Spectra were taken using a 40x water immersion objective (NA=0.8), 0.20 mW laser power at the sample, and 1 s acquisition times. The error bars are the standard deviation observed from 6 separate measurements on different spots. A linear fit is plotted to show the expected trend in CN frequency with changes in applied potential.

To verify the formation of optically rectified fields on the surface of the Ag nanodendrites. The CN stretch mode was recorded with increasing laser power. Figure 2A shows the observed change in the CN frequency observed with increased laser power. The CN stretch frequency was determined from the center of a Gaussian line shape fit to the observed spectrum. The experiment was performed with 4 measurements from different spots on the same substrate.

From Eq. 1, we observe the expected linear change in frequency with increased power arising from a linear change in V_{DC}. The power range examined is limited by the output of our HeNe laser and the damage threshold of the surface. Over the 4.5 mW range measured, we observe a frequency shift of -0.32 cm^{-1} mW^{-1}. Figure 2B shows the spectra observed at 0.04 mW and 4.45 mW excitation power. The peaks are clearly shifted but show negligible broadening. The lack of broadening suggests that temperature is not a dominant factor at these powers, as temperature should increase the heterogeneous line broadening and give rise to wider peaks. Temperature is not expected to change the vibrational frequency of the CN moiety.

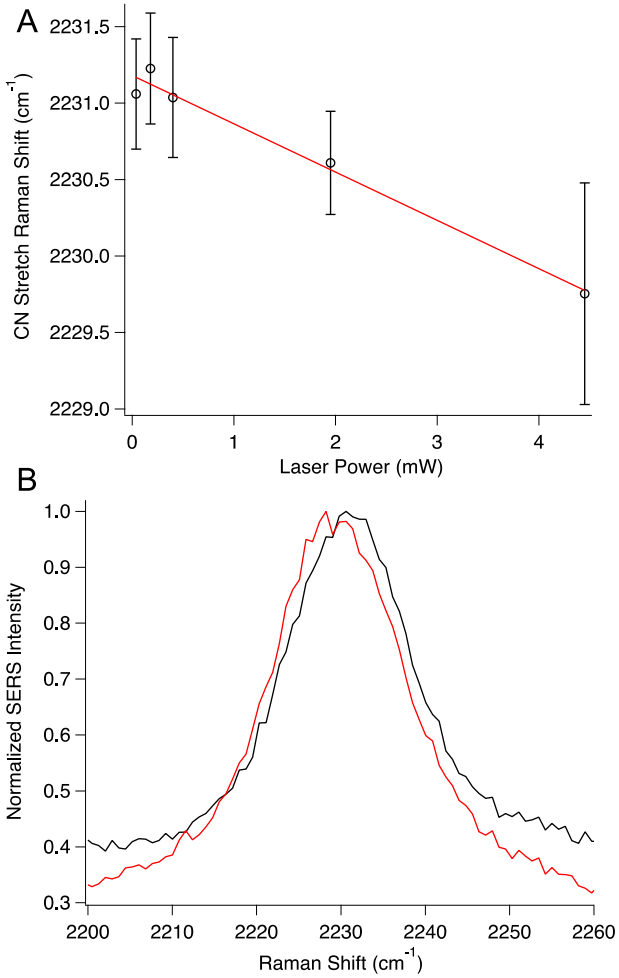

Figure 2. A) The CN stretch frequency is plotted as a function of laser power incident on a MBN functionalized Ag nanodendrite surface. With increasing power, the CN stretch is observed at decreasing Raman shifts. The change in Raman shift with power indicates the formation of a negatively charged optically rectified field on the electrode surface. B) Example spectra obtained at 0.04 mW (black) and 4.45 (red) are shown. The spectra were corrected for acquisition time and laser power and then normalized for comparison. Spectra were obtained using a 50x air objective (NA=0.75)

The results in Figures 1 and 2 combine to suggest that the plasmonic structures give rise to a negatively charged surface with increasing laser power. This negative potential should affect the reduction and oxidation activity on the electrode surface. To assess the impact of the optically rectified electric fields on the electrochemical activity of the surface, spectro-electrochemical measurements were performed consisting of cyclic voltammetry in the presence of 2mM $CuSO_4$ while the surface was either illuminated with a 565 nm LED or dark. Figure 3 shows results from these spectro-electrochemical measurements. In the absence of illumination, Figure 3A shows that as the potential is made more negative, a reduction peak is observed near -0.05 V. Upon switching the direction of the potential sweep, two oxidation peaks are observed at 0.05 V and 0.2 V. There is some minor fluctuation of the peaks, likely arising from inhomogeneities on the highly branched electrodes. When the surface is illuminated with the diode, a new reduction peak is observed at 0.1 V in the cathodic sweep, and

at 0.25 V upon switching the potential in the anodic sweep. The peak currents associated with these new peaks are observed to diminish and disappear when the light is turned off.

Figure 3B shows the time dependent behavior observed from the photo-induced peaks on the surface. The reduction and oxidation peak currents are shown to correlate with illumination of the surface. The increase and decrease in peak current occurs on a timescale of seconds, suggesting that mass transport effects (e.g. double-layer charging) impact the formation of the optically rectified fields on the electrode surface. Further study is needed to explore the origins of the observed kinetics. However, the new oxidation and reduction peaks are observed at potentials positive of the events measured in the dark. This is consistent with optical rectification providing an increase in negative potential to facilitate these electrochemical transitions.

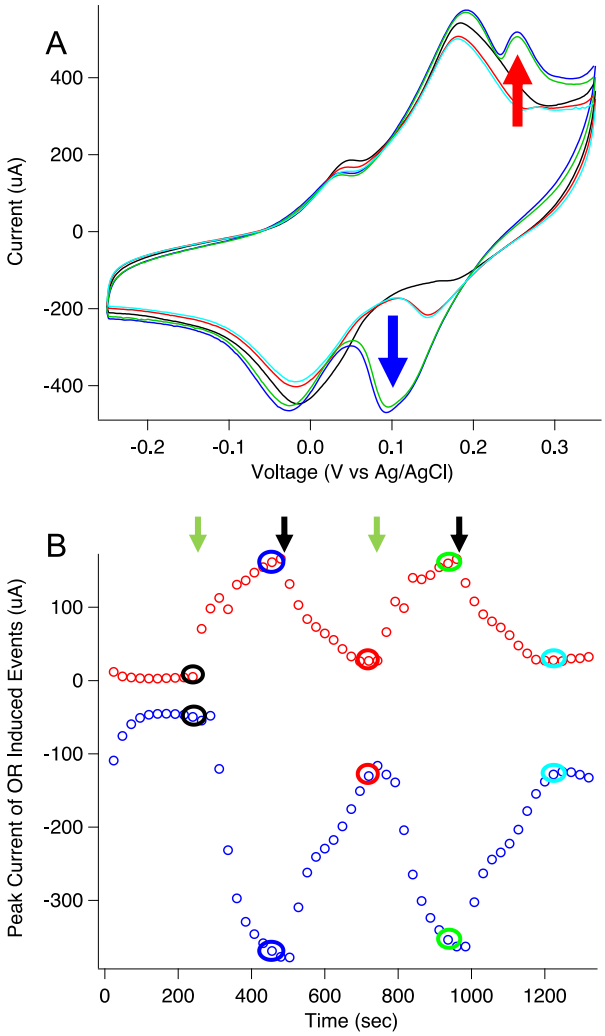

Figure 3. A) Cyclic voltammograms taken with and without illumination from 565 nm LED are shown. When the Ag plasmonic electrode is illuminated, new peaks are observed in the cathodic wave (blue arrow) and anodic wave (red arrow). B) The samples peak current of the photo induced voltammogram peaks (red and blue) are plotted versus time. When the LED is turned on is noted by the green arrow, while the time when the LED is turned off is noted by the black arrow. The colored circles correspond to the similarly colored voltammograms in (A).

To further examine the origins of the photo-induced electrochemical behavior we obtained Raman images of the MBN functionalized surface with and without diode illumination (Figure 4). To avoid interference from the diode in our Raman measurements, we used a 455 nm LED with an estimated power density of 5.4 mW/mm^2. The Raman excitation laser power was minimized to 0.008 mW to avoid inducing an additional Stark shift. From Figure 2, this laser power has a negligible impact on the CN stretch frequency. Figure 4A plots the CN stretch frequency observed from a Ag dendrite SERS surface without LED illumination. Similar to previous results, the magnitude of the CN shift is observed to distribute across different regions of the substrate.

In Figure 4B, we observe that LED illumination produces a change in the observed CN stretch frequencies. By repeating the Raman map with the LED illuminating this region, the value of the CN stretch is observed to increase in some areas and decrease in others. Using the Stark tuning coefficient (8 cm^{-1}/ V) determined from Figure 1, we are able to determine the distribution of surface potentials on the nanostructured silver surface. The intensities observed in the repeated Raman maps were consistent, indicating no visible drift or photodamage occurred. The observed CN stretch frequencies were observed to change.

Figure 4C plots the distribution of surface potentials observed from 3 different experiments. To create the distribution, a linear background was subtracted and the spectra fit to a single Gaussian lineshape. Only peaks 3 standard deviations above the noise were included. The observed frequencies were weighted by the fit amplitude. The change in Raman shift was then converted to surface potential using the Stark tuning coefficient determined in Figure 1. The mean calculated surface potential of -0.054 V agrees with the observed center of the Gaussian distribution of -0.052 V; however, it is evident that there are regions with substantially different charge.

The small net change in surface charge helps explain the new peaks observed in the cyclic voltammetry experiments. If the optically rectified fields altered the surface potential of the entire surface, the applied electrochemical potential relative to Ag/AgCl would shift proportionally. However, with illumination, we observe two distinct behaviors: one representative of the electrode in the dark, and two a photo-induced behavior requiring less overpotential to drive the electrochemical reaction. Based on the distributions in Figure 4C, we assign the photo-induced behavior to those areas that have significantly shifted surface potentials. The ~150 mV shift in peak potential observed in the CV experiment is easily contained in the distribution of potentials in Figure 4C. Previous work has associated defects, step edges, and nanoparticle corners as catalytically active sites,[10, 11] this agrees with our observations. However, we believe the optically rectified field at these sites also plays a role in the observed photo-electrochemical activity.

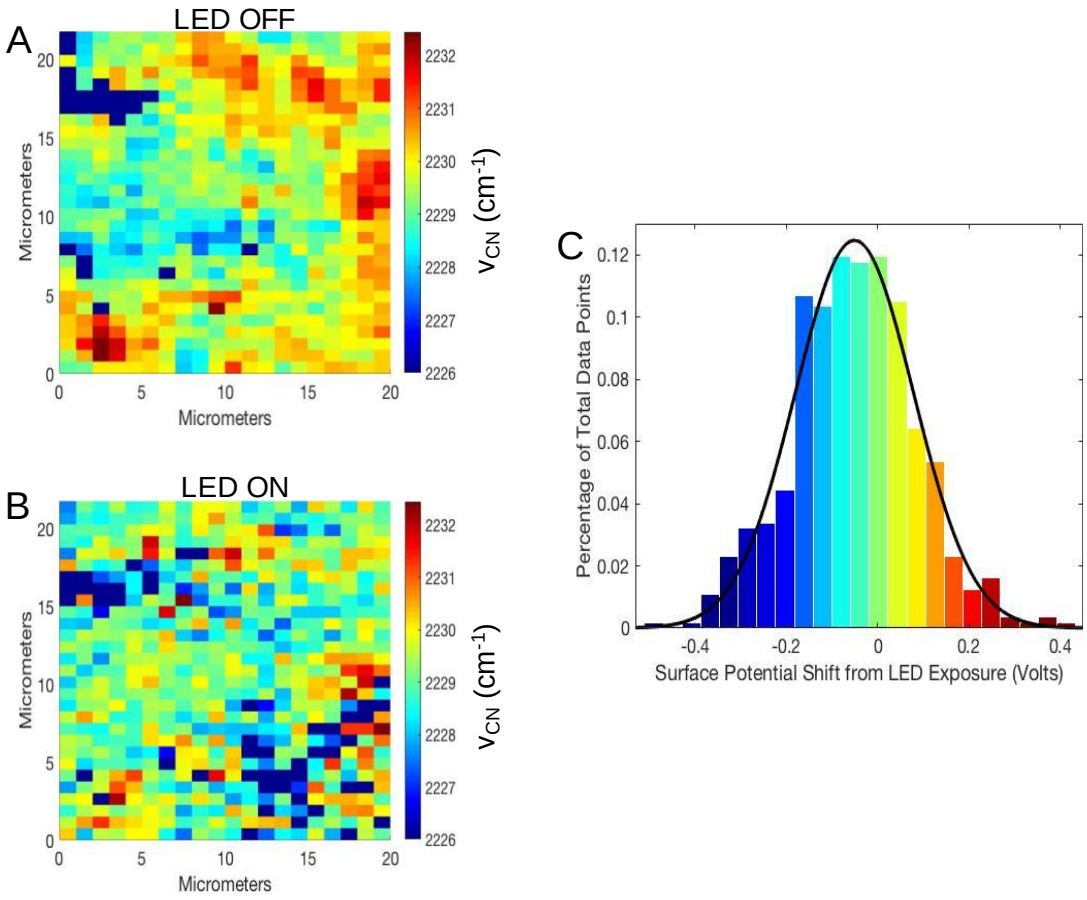

Figure 4. A) The image plots the CN stretch frequency observed from an MBN functionalized surface without LED illumination. B) Changes in the CN frequency over the same area plotted in (A) are observed when a 455 nm LED illuminates the surface at power density of 5.4 mW/mm^2. C) The difference in CN stretch frequency with and without illumination at each pixel in 3 separate experiments were combined and converted to surface potential using the Stark tuning coefficient (8 cm^{-1}/V) determined in Figure 1. The black line is the Gaussian fit to the distribution.

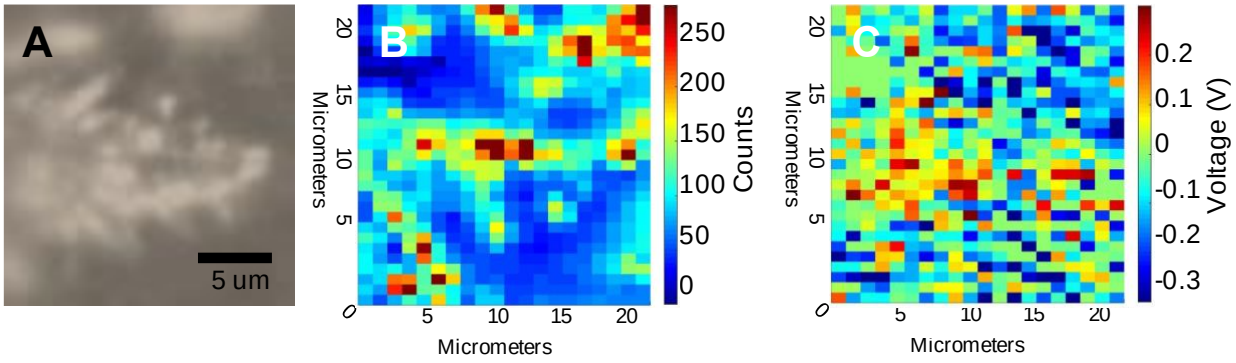

Figure 5. The brightfield image of the Ag dendrite (A) and the corresponding Raman map (B) plotted from the intensities of the CN stretch are shown. C) The distribution of surface potentials calculated from the change in CN stretch frequency with and without illumination

for the Raman map (B) provides a far field picture of how the change in charge density corresponds to the location of hotspots. In (C), red indicates a more positive, blue is a more negative, and green is unchanged surface potential.

To further evaluate the correspondence between "hotspots" and the observed optically rectified fields, Figure 5 shows how the SERS intensity corresponds with the observed distribution of surface potentials. Figure 5A shows the brightfield image of the Ag dendrite surface corresponding to the Raman map in Figure 5B. In Figure 5B, the intensity of the CN stretch from the MBN molecules on the Ag dendrite is plotted. Regions of intense Raman scattering are observed along the dendrites. Figure 5C shows the calculated charge distribution from the same area determined from maps with and without illumination. The correlation between the hotspots and the charge density is not clear. However, this is reasonable because the hotspots, nanojunctions, are the point where the electrons tunnel between nanostructures. Therefore, one side should be positively charged and the other negatively charged. The Raman microscopy used in this experiment does not have the spatial resolution to distinguish spectroscopic changes on this length scale. What is observed are pockets of altered charge density near where hotspots are observed. The physical structures that correlate to these pockets of altered charge density are hypothesized to give rise to the photo-induced features in the cyclic voltammetry.

SUMMARY AND CONCLUSIONS

Taken together our results suggest optical rectification of plasmonic fields are relevant to catalytic reactions on these materials. Figure 6 summarizes our results and presents a picture of what we believe may occur. In the presence of light to drive the plasmon resonance, electrons can tunnel though nanojunctions and give rise to optically rectified fields (V_{DC}). This optically induced voltage raises the Fermi level of the electrode in localized regions. These localized fields on the plasmonic material enable electrochemical reactions at reduced overpotentials. In Figure 6, we analyze the cathodic wave of the CV, which appears to have more straightforward behavior. $E_{p,c}$ corresponds to the reduction of Cu by the electrode without the assistance of the plasmon. When the plasmons are excited, regions on the electrode at increased negative potential drive the reaction at lower applied potential giving rise to $E_{p,c}$*. The behavior of the anodic wave is also consistent with this explanation; however, the two oxidation peaks observed in the dark require additional treatment.

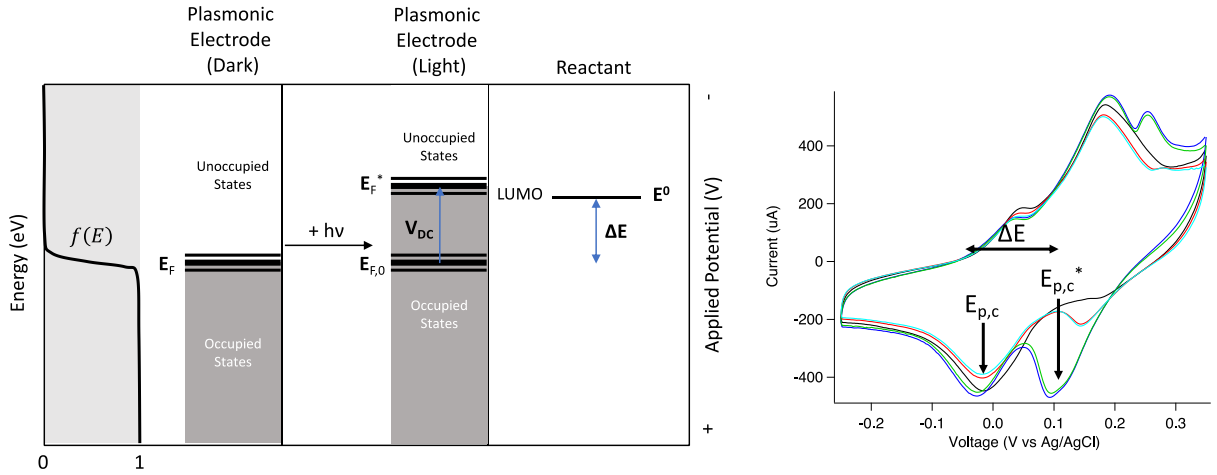

Figure 6. The schematic illustrates the connection between the optically rectified field (V_{DC}) and the observation of new redox peaks in the CV measurement. $E_{p,c}$ is the reduction peak arising from the regions of the electrode that show no change in potential with optical illumination and have electrons with a defined Fermi level ($E_{F,0}$). $E_{p,c}$* corresponds to regions of the electrode where the optically rectified field (V_{DC}) raises the energy of the Fermi level, enabling reduction with less applied negative potential.

This model has implications for mechanisms of plasmonic catalysis. First, no thermal effects are included in this model. Our observations are based on changes in, and indicators of, potential. Both the frequency of bond and the redox peak observed in CV are expected to broaden at increased temperature, but not shift. The Fermi-Dirac distribution of electrons into different energy levels, f(E), is sensitive to temperature, but the center of the distribution, the Fermi level, does not change. While temperature clearly has an effect on catalytic rates, it is in addition to the optically rectified fields. Second, our previous work indicates that nanojunctions are required for optical rectification.[19] This suggests that reactions on isolated plasmonic structures occur through a different mechanism, such as hot electron generation. In the case of coupled nanostructures, the optically rectified field has been shown to modulate the hot electron associated reaction rates.[22]

In conclusion, the combination of Stark spectroscopy and electrochemical measurement provides evidence that optical rectification on plasmonic surfaces plays an important role in plasmon catalysis. Future efforts to design catalytic materials will benefit from understanding the impact of this nonlinear process.

ACKNOWLEDGMENT

The authors acknowledge Dr. Rafael Masitas for his input on using Ag dendrites for a SERS substrate. This work was supported by the National Science Foundation award CHE-1830994.

REFERENCES

1. S. Linic, P. Christopher and D. B. Ingram, *Nature Materials*, 2011, **10**, 911-921.
2. P. Christopher, H. L. Xin and S. Linic, *Nat. Chem.*, 2011, **3**, 467-472.
3. Y. C. Zhang, S. He, W. X. Guo, Y. Hu, J. W. Huang, J. R. Mulcahy and W. D. Wei, *Chem. Rev.*, 2018, **118**, 2927-2954.
4. S. Navalon, M. de Miguel, R. Martin, M. Alvaro and H. Garcia, *J. Am. Chem. Soc.*, 2011, **133**, 2218-2226.
5. H. Y. Zhu, X. B. Ke, X. Z. Yang, S. Sarina and H. W. Liu, *Angewandte Chemie-International Edition*, 2010, **49**, 9657-9661.
6. X. Chen, Z. F. Zheng, X. B. Ke, E. Jaatinen, T. F. Xie, D. J. Wang, C. Guo, J. C. Zhao and H. Y. Zhu, *Green Chem.*, 2010, **12**, 414-419.
7. X. Chen, H. Y. Zhu, J. C. Zhao, Z. T. Zheng and X. P. Gao, *Angewandte Chemie-International Edition*, 2008, **47**, 5353-5356.
8. S. J. Yu, A. J. Wilson, J. Heo and P. K. Jain, *Nano Lett*, 2018, **18**, 2189-2194.
9. X. Zhang, X. Q. Li, D. Zhang, N. Q. Su, W. T. Yang, H. O. Everitt and J. Liu, *Nat. Commun.*, 2017, **8**, 1-9.
10. L. Kubus, H. Erdogan, S. S. Cetin, E. Biskin and G. Demirel, *Chemcatchem*, 2013, **5**, 2973-2977.
11. J.-H. Zhong, X. Jin, L. Meng, X. Wang, H.-S. Su, Z.-L. Yang, C. T. Williams and B. Ren, *Nat Nano*, 2017, **12**, 132-136.
12. N. J. Halas, S. Lal, W. S. Chang, S. Link and P. Nordlander, *Chem. Rev.*, 2011, **111**, 3913-3961.
13. P. L. Stiles, J. A. Dieringer, N. C. Shah and R. R. Van Duyne, *Annu Rev Anal Chem*, 2008, **1**, 601-626.
14. P. K. Jain, X. H. Huang, I. H. El-Sayed and M. A. El-Sayed, *Accounts Chem. Res.*, 2008, **41**, 1578-1586.
15. L. Brus, *Accounts Chem. Res.*, 2008, **41**, 1742-1749.
16. J. Jiang, K. Bosnick, M. Maillard and L. Brus, *J. Phys. Chem. B*, 2003, **107**, 9964-9972.
17. Z.-C. Zeng, H. Wang, P. Johns, G. V. Hartland and Z. D. Schultz, *The Journal of Physical Chemistry C*, 2017, **121**, 11623-11631.
18. E. L. Keller and R. R. Frontiera, *ACS Nano*, 2018, **12**, 5848-5855.
19. H. Wang, K. Yao, J. A. Parkhill and Z. D. Schultz, *Physical Chemistry Chemical Physics*, 2017, **19**, 5786-5796.
20. D. T. Kwasnieski, H. Wang and Z. D. Schultz, *Chem Sci*, 2015, **6**, 4484-4494.
21. J. M. Marr and Z. D. Schultz, *The Journal of Physical Chemistry Letters*, 2013, **4**, 3268-3272.
22. D. A. Nelson and Z. D. Schultz, *J. Phys. Chem. C*, 2018, **122**, 8581-8588.
23. M. Banik, P. Z. El-Khoury, A. Nag, A. Rodriguez-Perez, N. Guarrottxena, G. C. Bazan and V. A. Apkarian, *ACS Nano*, 2012, **6**, 10343-10354.
24. V. Oklejas and J. M. Harris, *Appl. Spectrosc.*, 2004, **58**, 945-951.
25. V. Oklejas, C. Sjostrom and J. M. Harris, *J. Am. Chem. Soc.*, 2002, **124**, 2408-2409.
26. D. K. Lambert, *Electrochimica Acta*, 1996, **41**, 623-630.
27. S. A. Sorenson, J. G. Patrow and J. M. Dawlaty, *J. Am. Chem. Soc.*, 2017, **139**, 2369-2378.
28. J. G. Patrow, S. A. Sorenson and J. M. Dawlaty, *J. Phys. Chem. C*, 2017, **121**, 11585-11592.
29. A. J. Stafford, D. L. Ensign and L. J. Webb, *J. Phys. Chem. B*, 2010, **114**, 15331-15344.
30. S. G. Boxer, *J. Phys. Chem. B*, 2009, **113**, 2972-2983.
31. L. J. Webb and S. G. Boxer, *Biochemistry*, 2008, **47**, 1588-1598.

32. I. T. Suydam and S. G. Boxer, *Biochemistry*, 2003, **42**, 12050-12055.
33. W. H. Hu and L. J. Webb, *J. Phys. Chem. Lett.*, 2011, **2**, 1925-1930.
34. W. A. Bryan, C. R. Calvert, R. B. King, J. B. Greenwood, W. R. Newell and I. D. Williams, *Faraday Discuss.*, 2011, **153**, 343-360.
35. S. Y. Zou, Q. H. Ren, G. G. Balint-Kurti and F. R. Manby, *Phys. Rev. Lett.*, 2006, **96**.
36. K. Hermansson and H. Tepper, *Molecular Physics*, 1996, **89**, 1291-1299.
37. D. R. Ward, F. Huser, F. Pauly, J. C. Cuevas and D. Natelson, *Nature nanotechnology*, 2010, **5**, 732-736.
38. Y. R. Shen, *The principles of nonlinear optics*, J. Wiley, New York, 1984.
39. R. Esteban, A. G. Borisov, P. Nordlander and J. Aizpurua, *Nat. Commun.*, 2012, **3**, 825.
40. K. J. Savage, M. M. Hawkeye, R. Esteban, A. G. Borisov, J. Aizpurua and J. J. Baumberg, *Nature*, 2012, **491**, 574-577.
41. V. Oklejas, C. Sjostrom and J. M. Harris, *J. Phys. Chem. B*, 2003, **107**, 7788-7794.
42. G. L. Beltramo, T. E. Shubina, S. J. Mitchell and M. T. M. Koper, *Journal of Electroanalytical Chemistry*, 2004, **563**, 111-120.
43. A. T. Sage, J. D. Besant, B. Lam, E. H. Sargent and S. O. Kelley, *Accounts Chem. Res.*, 2014, **47**, 2417-2425.
44. A. Gutes, C. Carraro and R. Maboudian, *J. Am. Chem. Soc.*, 2010, **132**, 1476-+.